SPECIAL TOPIC — Optical field manipulation

Creation of topological vortices using Pancharatnam–Berry phase liquid crystal holographic plates*

Xuyue Guo(郭旭岳), Jinzhan Zhong(钟进展), Peng Li(李鹏)†, Bingyan Wei(魏冰妍)‡, Sheng Liu(刘圣), and Jianlin Zhao(赵建林)

MOE Key Laboratory of Material Physics and Chemistry under Extraordinary Conditions, and Shaanxi Key Laboratory of Optical Information Technology, School of Physical Science and Technology, Northwestern Polytechnical University, Xi'an 710129, *China*

(Received 7 January 2020; revised manuscript received 9 February 2020; accepted manuscript online 20 February 2020)

Recently, physical fields with topological configurations are evoking increasing attention due to their fascinating structures both in fundamental researches and practical applications. Therein, topological light fields, because of their unique opportunity of combining experimental and analytical studies, are attracting more interest. Here, based on the Pancharatnam–Berry (PB) phase, we report the creation of Hopf linked and Trefoil knotted optical vortices by using phase-only encoded liquid crystal (LC) holographic plates. Utilizing scanning measurement and the digital holographic interference method, we accurately locate the vortex singularities and map these topological nodal lines in three-dimensions. Compared with the common methods realized by the spatial light modulator (SLM), the phase-only LC plate is more efficient. Meanwhile, the smaller pixel size of the LC element reduces the imperfection induced by optical misalignment and pixellation. Moreover, we analyze the influence of the incident beam size on the topological configuration.

Keywords: topological vortices, Pancharatnam–Berry phase, liquid crystal, phase singularity, hologram

PACS: 03.65.Vf, 42.79.Hp, 42.40.Eq, 42.70.Df **DOI:** 10.1088/1674-1056/ab7805

1. Introduction

With the development of laser technology in various realms, exploring light fields with ingenious spatial structures and intriguing evolution features is becoming a hot spot of optics and photonics. In recent years, optical vortices carrying orbital angular momenta (OAM) and two-dimensional phase singularities have drawn extensive attention and been exploited in various applications, including optical imaging,[1,2] particles manipulation,[3,4] optical information storage,[5] communication,[6,7] and so on.[8–10] Recently, a special kind of optical fields, whose vortex singularities are three-dimensionally connected as isolated loops in the forms of topological configurations such as vortex knots and links,[11–15] has aroused great concerns.

Since the theoretical proposal of Lord Kelvin,[16] the knots and links have been demonstrated playing a fundamental role in a wide range of physical branches such as plasmas,[16,17] quantum field,[18] classical fluid,[19,20] and liquid crystals.[21,22] In optical regime, the model in which the vortex lines (connected vortex singularities) can be knotted or linked and show topological structures was first theoretically reported by Berry and Dennis in 2001,[23] and experimentally constructed by Leach *et al.* based on the linear superposition of Laguerre–Gaussian (LG) beams with optimized intensities and phases.[24,25] Such vortex lines in light fields can be potentially applied as a topological waveguide for quantum mechanical matter waves, such as Bose–Einstein condensates.[26,27] Furthermore, because the light fields exhibit an unique opportunity of combining experimental and analytical studies, the optical topology is attracting more attention for studying topological fields and furthermore understanding the common topological configurations in disparate matter systems. To precisely create topological vortices, the holographic reconstruction based on a spatial light modulator (SLM) is a common approach. However, for this method, the disadvantages induced by the relatively large pixel size of the SLM, such as misalignment and pixellation, limit the construction perfection. Therefore, an efficient optical device with smaller pixel is necessary to overcome such issues.

In this paper, we report the creation of topological vortices by using liquid crystal (LC)[28] holographic Pancharatnam–Berry (PB) phase[29,30] plates fabricated via sulphonic azo-dye SD1 based photoalignment technology and digital micro-mirror device (DMD) based dynamic exposure process. The continuous orientation of the LC molecules in such a PB phase plate reduces the imperfection arising from pixelated SLM, allowing the precise reconstruction of

*Project supported by the National Natural Science Foundation of China (Grant Nos. 11634010, 91850118, 11774289, 61675168, and 11804277), the National Key Research and Development Program of China (Grant No. 2017YFA0303800), the Joint Fund of the National Natural Science Foundation of China and the China Academy of Engineering Physics (Grant No. U1630125), and the Fundamental Research Funds for the Central Universities, China (Grant Nos. 3102018zy036, 3102019JC008, and 310201911cx022).

†Corresponding author. E-mail: pengli@nwpu.edu.cn

‡Corresponding author. E-mail: wbyxz@nwpu.edu.cn

three-dimensional (3D) vortex singularities, namely, topological vortices. Moreover, we adopt the scanning measurement and the digital holographic interference methods to accurately map the topological configurations, locating the vortex singularities in 3D space. These designed LC plates with high performance provide a way to extend further fundamental study and applications of topological vortices.

2. Design and experiment

To design and fabricate LC plates, we start from the configuration of isolated topological structures. The common realization method is the linear superposition of LG fields with optimized coefficients and beam widths according to the Milnor polynomials.[25] Theoretically, considering the 3D topological field as a solution of the Helmholtz equation, we decompose the topological fields at the $z=0$ plane into multiple LG fields, i.e., $\psi = \Sigma a_i \mathrm{LG}_p^l(w)$. Wherein $\mathrm{LG}_p^l(\cdot)$ denotes the LG fields characterized by indices $(l,\ p)$, with l and p corresponding to the azimuthal and radial indices, respectively, a_i is the coefficient of the LG field, and w denotes the waist width that determines the 3D scale of the isolated topology. Here, we select the Hopf link and Trefoil knot as topology examples,[11] as shown in Figs. 1(a) and 1(b). After the optimization of the coefficients, the corresponding fields at the $z=0$ plane can be expressed as

$$\begin{aligned}\psi_{\mathrm{link}} &= -6.32\mathrm{LG}_1^0(1.4)+4.21\mathrm{LG}_2^0(1.4)\\ &\quad -5.95\mathrm{LG}_0^2(1.4)+2.63\mathrm{LG}_0^0(1.4),\\ \psi_{\mathrm{knot}} &= -5.66\mathrm{LG}_1^0(1.2)+6.38\mathrm{LG}_2^0(1.2)-2.3\mathrm{LG}_3^0(1.2)\\ &\quad -4.36\mathrm{LG}_0^3(1.2)+1.71\mathrm{LG}_0^0(1.2),\end{aligned} \tag{1}$$

whose amplitude and phase distributions are shown in Figs. 1(c) and 1(d).

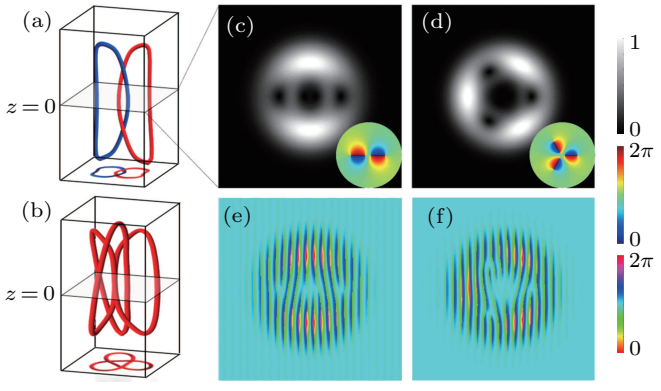

Fig. 1. (a), (b) The 3D views of isolated Hopf link and Trefoil knot. (c), (d) The amplitude and phase (insets) distributions of the Hopf linked and Trefoil knotted fields at the beam waist ($z=0$) plane. (e), (f) Phase-only holograms generated by the inverse sinc functional phase-only encoding technique corresponding to the Hopf linked and Trefoil knotted fields.

In order to simultaneously control the amplitude and phase of the light fields shown in Eq. (1), we use the efficient phase-only hologram. To generate a phase-only hologram, we employ the inverse-sinc functional phase-only encoding technique[31] to encode the amplitude profile as a mask into the phase function. For this scheme, the target field can be obtained from the first-order spatial spectrum. Figures 1(e) and 1(f) show the phase-only holograms corresponding to the linked and knotted fields, respectively.

Next, we map the holograms into LC plates by using sulphonic azo-dye SD1 based photoalignment technology and DMD based microlithography system[32,33] with a spatial resolution of 1.08 μm×1.08 μm. Via an eighteen-step five-time-partly-overlapping exposure process,[34,35] a director variant LC PB phase plate can thus be formed. The corresponding polarized optical microscopic images are shown in Figs. 2(a) and 2(b), respectively. It can be seen that the structures of these samples match well with Figs. 1(e) and 2(f). Consequently, such LC elements will impose PB phases expressed as $\pm 2\theta$ onto the transmitted field under the illumination of left/right-handed circular polarization.[36] Wherein $\theta = \Phi/2$ is the orientation angle of the LC directors according to the phase function Φ, and $\pm$ are the phase shift symbols introduced for the incident left- and right-handed circular polarizations, respectively. Thanks to the excellent electro-optical properties of LCs, this device can operate over a wide range of spectrum.[7,37,38] However, according to the inverse-sinc encoding principle, the phase retardation depth will influence the ratio of the first order component. This means that for an unmatched wavelength (birefringent retardation is not equal to π), the generation efficiency would be reduced.

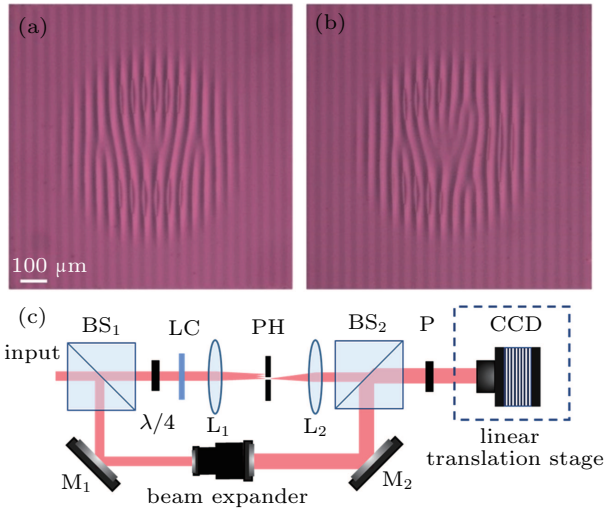

Fig. 2. (a), (b) Micrographs of fabricated LC holographic plates corresponding to Hopf link and Trefoil knot, respectively. The sizes of the pattern areas are both 1 mm×1 mm. (c) Experimental setup for configuring and detecting vortex links and knots. The CCD is fixed on a linear translation stage to implement the scanning of the output field along z direction. BS_1 and BS_2, beam splitters; L_1 and L_2, lenses; M_1 and M_2, mirrors; PH, pinhole; P, polarizer; LC, liquid crystal holographic plates; $\lambda/4$, quarter wave plate.

The experimental setup to observe the topological vortices generated from the LC plates is shown in Fig. 2(c). In experiments, the input linearly polarized Gaussian beam (He–Ne laser, 633 nm) is firstly split into two constituents by a beam splitter (BS_1). The reflected constituent is expanded by a beam expander and used as a reference beam. The transmitted one is incident on the LC plate after passing through a quarter wave plate, which is used to adjust the polarization state of the input beam. The transmitted beam imposed with desired phase then passes through a $4f$ filter system consisting of two lenses (focal lengths are both 15 cm) and a pinhole (PH) with only the first diffractive order passing through. The transmitted order finally overlaps with the reference constituent via the BS_2. At the back focal plane of the $4f$ system, where we define as the $z = 0$ plane, we can observe the light fields corresponding to the distributions of the linked and knotted fields at the beam waist plane. The polarizer (P) is used to adjust the polarization state to obtain a high quality interferogram, and the charge-coupled device (CCD, pixel size is 3.75 μm×3.75 μm) is fixed on a linear translation stage along the z direction, allowing a 3D scan of the output field.

3. Results

Figure 3(a) shows the interferogram of the Hopf linked field and the reference field recorded at $z = 0$ plane, and figures 3(b) and 3(c) display the amplitude and phase distributions demodulated from the interferogram by the digital holography.[39] Clearly, compared with the target field shown in Fig. 1(c), the experimental results are consistent well with the theory. According to this phase distribution, we further accurately locate the phase singularities by utilizing a special algorithm,[40] which separates these points from the background by means of the high frequency characteristics of phase singularity. In contrast to the traditional overexposure intensity method,[25,41] which locates the phase singularities through an optimization algorithm of the intensity darkness, our method is simple and accurate. The four dark points mapped in Fig. 3(d) depict the locations of the phase singularities obtained by this method. The corresponding results of the Trefoil knotted field are shown in Figs. 3(e)–3(h).

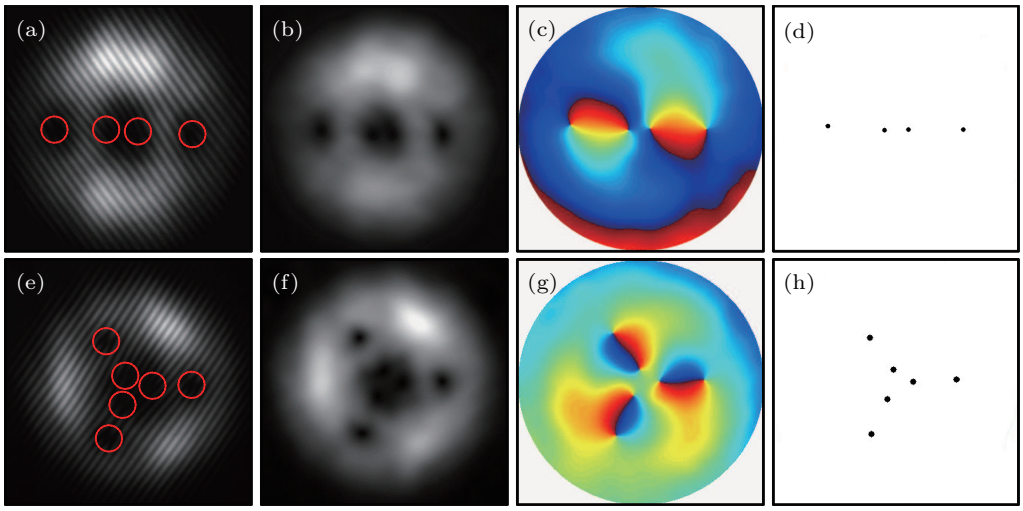

Fig. 3. (a), (e) Interferograms of the Hopf linked and Trefoil knotted fields with the reference field recorded at the $z = 0$ plane, respectively. (b), (f) Intensity and (c), (g) phase distributions reconstructed from the interferograms. (d), (h) Phase singularities mapped by the location algorithm based on the spatial spectrum of the phase pattern.

Further, we measure the distribution of phase singularities in 3D space by scanning different planes along the z direction.[40] The left charts of Figs. 4(a) and 4(b) show the phase singularity locations of the Hopf link and Trefoil knot in five different x–y planes, respectively. It is clear that, in Fig. 4(a), two singularities appear in the z_1 plane, indicating that four vortex lines connect into two loops at this plane. Comparing with the overexposure intensity method, this algorithm provides precise separate points, instead of wide low-intensity regions in the plane near the inflexion of the vorticity lines. It should be noted that, in Fig. 4(b), these six phase singularities in the Trefoil knot are not composited simultaneously at the same plane, as five singularities appear in this plane, due to experimental errors such as beam tilt or air disturbance. By connecting these phase singularities in 100 planes, isolated topological configurations are obtained as shown in the right charts of Figs. 4(a) and 4(b). For comparison, the theoretical configurations are shown in Figs. 4(c) and 4(d). Intuitively, intact Hopf link and Trefoil knot are successfully generated from the LC plates. The measured diameters of these configurations are about 660 μm, and the longitudinal lengths are about 10 cm. The generation efficiency is about 10%.

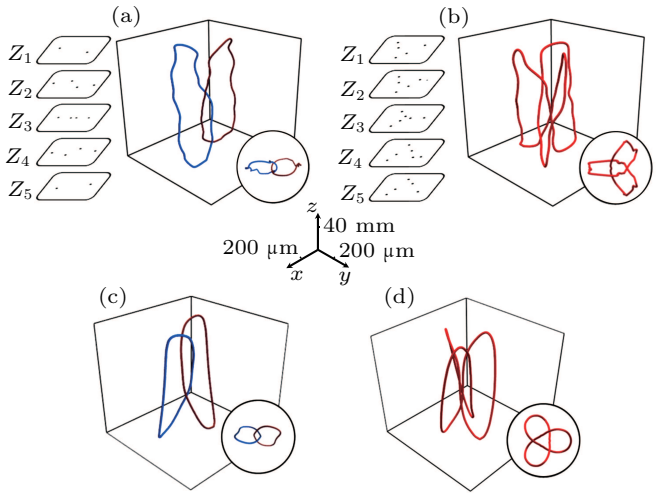

Fig. 4. (a), (b) Phase singularity locations at five different transverse planes and isolated Hopf link and Trefoil knot configured from the phase distributions measured by the scanning method. Insets: Top views of the topological configurations. The measured diameters of these configurations are about 660 μm, the longitudinal lengths are about 10 cm. (c), (d) Isolated Hopf link and Trefoil knot configured from numerical calculation.

4. Discussion

The above experimental results demonstrate the successful generation of topological vortices by using PB phase LC plates. Compared with the configurations constructed from SLM, here reported ones have smaller geometry and therefore enable the more perfect construction of the vortex links and knots. Actually, the geometric size of the topological configurations is directly dependent on the scale of the hologram. Here, the size advantage of the LC molecules enables the more perfect construction. Besides, it is noteworthy that, the incident beam waist can also affect the topological configurations. Therefore, we further explore the influence of the size of the incident beam on the constructed configuration. Figure 5 displays the numerically configured Hopf link under the illuminations of Gaussian beams with different waists. The hologram has a phase-only distribution as shown in Fig. 1(e).

Figure 5(a) corresponds to the incidence of a plane wave. An obvious vortex link is obtained because of the pre-modulated waist in the hologram shown in Eq. (1). It is clear that, with the decrease of the waist of the incident beam, extra vortex lines appear and come near the isolated vortex link. The isolated vortex link remains until the waist reduces to 6, and the geometric size of the vortex link does not change. With the further decrease of the incident beam waist, extra vortex lines reconnect with the isolated vortex lines gradually, and then the isolated topological link is broken. The configuration variation of the vortex line arises from the Gouy phase[42] of the LG field.[43,44] That is, with the decrease of the waist of the incident beam, the varying period of the z-dependent Gouy phases of the LG components consequently decreases, resulting in the longitudinal variation of the interference field and the vortex lines. From the above results, we can find that the configurations of the topological vortices generated from the PB phase LC plates are robust as long as the waist of the incident beam is big enough.

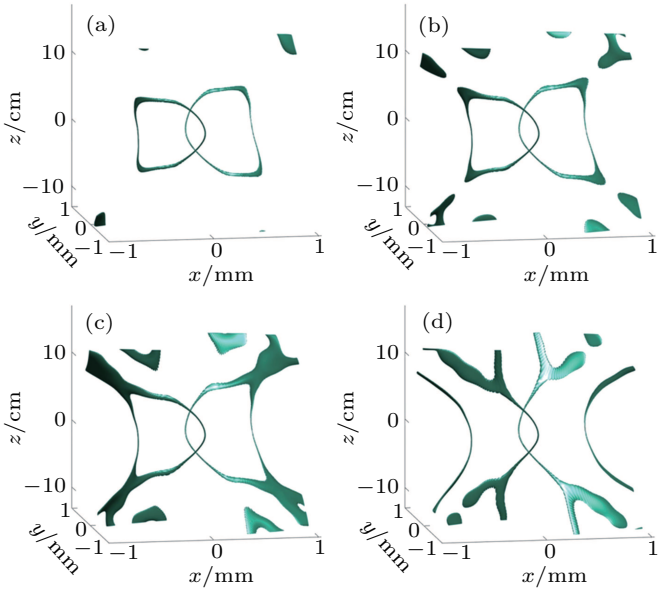

Fig. 5. Variation of 3D vortex lines with the decrease of the waist w_0 of the incident Gaussian beam: (a) $w_0 \to \infty$; (b) $w_0 = 8$; (c) $w_0 = 6$; (d) $w_0 = 4$. The vortex lines are mapped from the connection of phase singularities. w_0 is a normalized waist with respect to the pre-modulated w in Eq. (1).

5. Conclusion

We constructed two typical topological vortices of Hopf link and Trefoil knot via phase-only LC holographic plates, and accurately mapped the topological configurations by experimentally measuring the complex amplitude and phase distributions of 3D fields. Compared with the traditional methods using SLM, the PB phase LC plate has great advantages in size and cost, which ensures the generation quality and diversity. Moreover, the PB phase LC plate can operate in a wide spectrum range. This work supplies a versatile candidate for creating high quality topological vortices and may pave a way to extend further fundamental study and applications of topological vortices.

References

[1] Jack B, Leach J, Romero J, Franke-Arnold S, Ritsch-Marte M, Barnett S and Padgett M 2009 *Phys. Rev. Lett.* **103** 083602
[2] Fürhapter S, Jesacher A, Bernet S and Ritsch-Marte M 2005 *Opt. Express* **13** 689
[3] Friese M, Nieminen T, Heckenberg N and Rubinsztein-Dunlop H 1998 *Nature* **394** 348
[4] Zhao J, Chremmos I D, Song D, Christodoulides D N, Efremidis N K and Chen Z 2015 *Sci. Rep.* **5** 12086
[5] Chen P, Ge S J, Duan W, Wei B Y, Cui G X, Hu W and Lu Y Q 2017 *ACS Photon.* **4** 1333
[6] Zhao Y and Wang J 2015 *Opt. Lett.* **40** 4843
[7] Chen P, Ma L L, Duan W, Chen J, Ge S J, Zhu Z H, Tang M J, Xu R, Gao W and Li T 2018 *Adv. Mater.* **30** 1705865
[8] Li P, Wu D, Liu S, Zhang Y, Guo X, Qi S, Li Y and Zhao J 2018 *Chin. Phys. B* **27** 114201

[9] Han L, Liu S, Li P, Zhang Y, Cheng H and Zhao J 2018 *Phys. Rev. A* **97** 053802
[10] Zhang D, Cao X, Yang H, Gao J and Lv S 2019 *Chin. Phys. B* **28** 034204
[11] Dennis M R, King R P, Jack B, O'Holleran K and Padgett M J 2010 *Nat. Phys.* **6** 118
[12] Irvine W T and Bouwmeester D 2008 *Nat. Phys.* **4** 716
[13] Rañada A F 1989 *Lett. Math. Phys.* **18** 97
[14] Sugic D and Dennis M R 2018 *J. Opt. Soc. Am. A* **35** 1987
[15] Guo X, Li P, Zhong J, Liu S, Wei B, Zhu W, Qi S, Cheng H and Zhao J 2020 *Laser Photon. Rev.*
[16] Lord K 1867 *Philos. Mag.* **34** 15
[17] Berger M A 1999 *Plasma Phys. Contr. F.* **41** B167
[18] Witten E 1989 *Commun. Math. Phys.* **121** 351
[19] Moffatt H 1981 *J. Fluid. Mech.* **106** 27
[20] Ricca R L and Berger M A 1996 *Phys. Today* **49** 28
[21] Chen B G, Ackerman P J, Alexander G P, Kamien R D and Smalyukh I I 2013 *Phys. Rev. Lett.* **110** 237801
[22] Machon T and Alexander G P 2014 *Phys. Rev. Lett.* **113** 027801
[23] Berry M V and Dennis M R 2001 *Proc. R. Soc. A* **457** 2251
[24] Leach J, Dennis M R, Courtial J and Padgett M J 2004 *Nature* **432** 165
[25] Leach J, Dennis M R, Courtial J and Padgett M J 2005 *New J. Phys.* **7** 55
[26] Dutton Z and Ruostekoski J 2004 *Phys. Rev. Lett.* **93** 193602
[27] Ruostekoski J and Anglin J 2001 *Phys. Rev. Lett.* **86** 3934
[28] Wang L, Xiao R W, Ge S J, Shen Z X, Lü P, Hu W and Lu Y Q 2019 *Acta Phys. Sin.* **68** 084205 (in Chinese)
[29] Zhou H, Li Z K, Wang H Y, Chen H W, Peng X H and Du J F 2016 *Chin. Phys. Lett.* **33** 060301
[30] Liu J A, Tu J L, Lu Z L, Wu B W, Hu Q, Ma H H, Chen H and Yi X N 2019 *Acta Phys. Sin.* **68** 064201 (in Chinese)
[31] Davis J A, Cottrell D M, Campos J, Yzuel M J and Moreno I 1999 *Appl. Opt.* **38** 5004
[32] Wei B Y, Liu S, Chen P, Qi S X, Zhang Y, Hu W, Lu Y Q and Zhao J L 2018 *Appl. Phys. Lett.* **112** 121101
[33] Wang L, Ge S, Chen Z, Hu W and Lu Y 2016 *Chin. Phys. B* **25** 094222
[34] Chen P, Wei B Y, Ji W, Ge S J, Hu W, Xu F, Chigrinov V and Lu Y Q 2015 *Photon. Res.* **3** 133
[35] Wei B Y, Chen P, Hu W, Ji W, Zheng L Y, Ge S J, Ming Y, Chigrinov V and Lu Y Q 2015 *Sci. Rep.* **5** 17484
[36] Chen P, Wei B Y, Hu W and Lu Y Q 2019 *Adv. Mater.* **31** 1903665
[37] Wei B Y, Hu W, Ming Y, Xu F, Rubin S, Wang J G, Chigrinov V and Lu Y Q 2014 *Adv. Mater.* **26** 1590
[38] Chen P, Ma L L, Hu W, Shen Z X, Bisoyi H K, Wu S B, Ge S J, Li Q and Lu Y Q 2019 *Nat. Commun.* **10** 2518
[39] Liu S, Han L, Li P, Zhang Y, Cheng H and Zhao J 2017 *Appl. Phys. Lett.* **110** 171112
[40] Zhong J, Qi S, Liu S, Li P, Wei B, Guo X, Cheng H and Zhao J 2019 *Opt. Lett.* **44** 3849
[41] Maucher F, Gardiner S and Hughes I 2016 *New J. Phys.* **18** 063016
[42] Li P, Fan X, Wu D, Liu S, Li Y and Zhao J 2020 *Photon. Res.*
[43] Freund I 1999 *Opt. Commun.* **163** 230
[44] Siegman A E 1986 *Lasers* (Mill Valley: University Science Books)